Pulse electrodeposition of Ni/nano-SiC composite coatings: Effect of waveform, duty cycle and current density

Gholamreza Heidari[a*] & Mohammad Mosavie-Khoei[b]

[a]Esfarayen University of Technology, Esfarayen, North Khorasan, Iran
[b]Department of Mining and Metallurgy, Amir Kabir University of Technology, Tehran, Iran

In this study, nano-sized SiC particles have been codeposited with nickel using an additive free sulfamate bath under pulsed direct current (PDC) and direct current (DC). In order to find the effect of current density, duty cycle (D.C.) and waveform on coating, coatings have been studied in terms of microstructure, microhardness and SiC-codeposition. The scanning electron microscope results shown that the grain microstructure of the coatings have significantly affected by the waveform and D.C. changing the waveform in order of square, sine and ramp and also decreasing the D.C. resulted in finer grain microstructure. The SiC codeposition has shown an optimum value of about 3.3 wt% at the D.C. value of 30%; it also shows a reasonable trend with changes in the waveform. Moreover, according to the microhardness results, the composite coatings with fine grain microstructure have shown a higher microhardness.

Keywords: Electrodeposition, PDC, Waveform, Duty cycle, Current density

1 Introduction

Coating has been introduced as a common method to increase the service life by increasing the wear and corrosion resistance[1-3]. Electroplating is a cost effective and low temperature method for alloy electrodeposition[4, 5] and co-deposition of metallic and nonmetallic particles with metal matrix. Electroplating of metal matrix composite coatings with nano and micro particles such as TiO_2[6], CeO_2[7], ZrO_2[8, 9], Al_2O_3[10], SiC[11], WC[12, 13], CNT[14], Si_3N_4[15], Graphite[16], Graphene[17], Diamond[18], TiN[19] and PTFE[20] has been the subject of numerous preceding investigations. Nano scaled particles are of great interest for their better performance compared to micro-sized particles[15]. Nickel electroplated layer is a corrosion and wear resistant coating which can be improved by codeposition with nano-sized particles[1]. Ni-SiC composite coatings have been introduced as wear resistant coatings for protection of industrial products[21]. Previous investigations have proved the effect of electroplating parameters such as pH, temperature, stirring rate, additive, current type, current density, duty cycle (D.C.) and waveform besides particle parameters such as size and particle distribution in coating on wear and corrosion properties of coatings[22]. Gyftou et al. investigated the effect of the frequency and D.C. on the

microhardness, microstructure and texture of SiC-codeposited coatings and found higher incorporation percentages of pulsed direct current (PDC) compared to direct current (DC), and more SiC-codiposition with decreasing the D.C[23].

Hu et al. found that the Ni-SiC composites under the triangular waveform with higher current density led to finer grain microstructure and therefore to higher microhardness[24]. Although the PDC has been used in some previous investigations, it still needs to undergo further research. Moreover, the effect of ramp and sinusoidal waveforms has not been investigated in the published literature. In this paper, in order to have a better understanding of the PDC, the effect of the waveform (square, ramp and sinusoidal), current density and D.C. on the microstructure, SiC code position and microhardness of coatings was investigated.

2 Material and Methods

The sulfamate bath was prepared for electroplating experiments. The composition of the electroplating bath is detailed in Table 1. SiC nanoparticles were used to co-electrodeposite with nickel to provide composite coatings. The SiC nanoparticles were purchased and then characterized by transmission electron microscope (TEM, Philips Co.) and x-ray diffraction (XRD, Bruker D8). The aqueous

---

*Corresponding author (E-mail:g.heidari976@gmail.com)

Table 1 — The composition and condition of the electroplating bath.

Composition/Condition	Quantity
$Ni(SO_3NH_2)$	200 g/l
$NiCl_2$	10 g/l
H_3BO_3	30 g/l
Temperature	50 °C
pH	4

suspension of the SiC nanoparticles was prepared and stirred for 24 hours and then added to the sulfamate bath. The electroplating solution was stirred for 1 hour using a magnetic stirrer and then homogenized for 30 minutes ultrasonically. The 200 ml plating solution was prepared and agitated by the magnetic stirrer during electroplating to achieve homogeneous suspension. The pH value of the solution was controlled digitally. A structural steel (St12) ($30\times30\times1$ mm^3) was used as cathode and a similar-sized nickel plate was used as anode. Before electroplating, the substrate (cathode) was ground by 1200 grit SiC waterproof paper and then a sequence of cleaning was performed to remove contamination. Different electroplating periods were used to obtain the same thickness (40 μm). Electroplating coatings were obtained under the DC and PDC according to Fig. 1 and Tables 2, 3 and 4. Figure 1 shows schematically the waveforms used for code position under PDC. Tables 2, 3 and 4 indicate different electroplating conditions used for code position under PDC. The scanning electron micrograph was recorded by SEM XL30 and the amount of the code posited SiC particles was determined using energy dispersive spectroscopy (EDS) coupled with the SEM at 10× magnification as an average of five measurements. According to the EDS results, atomic percent of Si and Nickel was used to calculate weight percent of SiC based on Eq. (1), as follows:

$$\mathbf{wt\% \ SiC} = \frac{(\%at \ Si \times M_{Si} + \%at \ Si \times M_C)}{(\%at \ Si \times M_{Si} + \%at \ Si \times M_C) + (\%at \ Ni \times M_{Ni})} \times \mathbf{100\%}$$

…(1)

where, M_{Si}, M_C and M_{Ni} are the molar weight of silicon, carbon and nickel, respectively. The microhardness values were measured under 15 g load for 5 s. The final hardness value was an average of ten measurements.

3 Results and Discussion

Composite coatings were obtained by co-depositing of nickel and the SiC nanoparticles. The
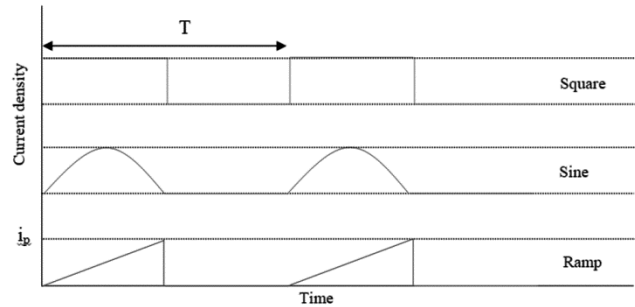

Fig. 1 — The schematic waveforms of the PDCs.

SiC nanoparticles were characterized by XRD and TEM. X-ray diffraction was used to confirm the purity of the SiC nanoparticles. As is obvious from Fig. 2, characteristic diffraction peaks of the SiC nanoparticles at 2θ values of 41.4, 48.1, 70.8, 85.5 and 89.9, respectively, corresponding to the reflections from the (104), (008), (201), (207), and (208) planes, were observed (Ref.code: 01-074-1302). The particle size of the SiC nanoparticles was obtained by TEM. According to the inset of Fig. 2, the average particle size of SiC was measured to be 40 nm.

3.1 Effect of Current Density on Microstructure, SiC-code position and Hardness

Figure 3 shows the SEM micrographs of the coatings produced by different current densities. Considering the SEM micrographs, it can be clearly observed that higher current density led to finer grain microstructure. This can be explained by the fact that as the current density increases, the nucleation rate increases in comparison with the grain growth and results in finer grain microstructure.

Figure 4 shows the variations in the amount of the code posited SiC particles in the coatings at different current densities. Increase in the SiC code position caused by changes in the current density was observed up to 6 A.dm^{-2}. Moreover, increase in current density resulted in higher reduction of ions surrounding the SiC particles so that higher amounts of the code posited SiC particles were obtained. As a result, it can be concluded that the code position process is charge transfer control up to 6A.dm^{-2}. Above 6A.dm^{-2}, the amount of the code posited SiC particles decreased with current density. Mobility of the nickel ions was more than that of the SiC particles; thus, higher amounts of the nickel ions can be reduced and deposited compared to the SiC particles. Accordingly, it can be deduced that above 6A.dm^{-2}, the SiC code position process is mass transfer control.

Table 2 — Electroplating variables of the PDC at different current densities.

Sample	Kind of current	Waveform	Current density, i_{max} (A.dm^{-2})	Duty cycle (%)	Frequency (Hz)
Square-2A	PDC	Square	2	50	100
Square-4A	PDC	Square	4	50	100
Square-6A	PDC	Square	6	50	100
Square-8A	PDC	Square	8	5	100

Table 3 — Electroplating variables of the PDC at different D.C.s and electroplating at the DC.

Sample	Kind of current	Waveform	Current density, i_{max} (A.dm^{-2})	Duty cycle (%)	Frequency (Hz)
Square-10dc	PDC	Square	4	10	100
Square-30dc	PDC	Square	4	30	100
Square-50dc	PDC	Square	4	50	100
Square-70dc	PDC	Square	4	70	100
DC-100dc	DC	--------	4	100	------

Table 4 — Electroplating variables of the PDC at different waveforms.

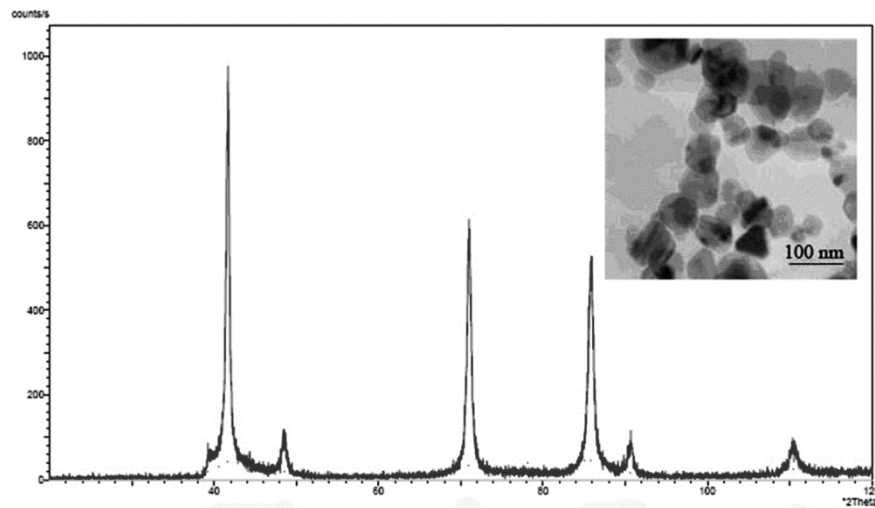| Sample	Kind of current	Waveform	Current density i_{max}	Duty cycle	Frequency
Square, Sine & Ramp	PDC	Square, Sine & Ramp	4 A.dm^{-2}	50%	100 Hz

Fig. 2 — The XRD pattern of the nano-sized SiC particles (Inset: The TEM image of the nano-sized SiC particles).

The microhardness results of the coatings at different current densities are shown in Fig. 4. As it is clearly shown, higher current density led to higher microhardness. Considering the SiC code position and microstructure, finer grain microstructure caused higher microhardness value. The microhardness of the coating increased to the current density value of 8A.dm^{-2}, albeit having lower SiC code position. Therefore decreasing the grain size is the main reason for increasing the microhardness value. It can be concluded that the Hall-Petch strengthening mechanism was dominant in the microhardness changes.

3.2 Effect of Duty Cycle (D.C.) on Microstructure, SiC-code position and Hardness

SEM micrographs of the coatings obtained at different D.C.s are shown in Fig. 5. The D.C. is defined according to Eq. (2) as follows:

$$D.C. = \frac{t_{on}}{t_{on} + t_{off}} \times 100\% \qquad \dots (2)$$

where, t_{on} and t_{off} denote the on-time and off-time periods of an electroplating cycle, respectively. As it is clearly observed, lower D.C. resulted in finer grain microstructure. This stems from the prohibition of the grain growth during the increased t_{off} period; thus, the decreased D.C. resulted in finer grains.

The SiC codeposition value obtained from electroplating with square waveform at different D.C.s is shown in Fig. 6. The results of square waveform are also compared with those of simple DC. It is observed that by increasing the D.C. up to 30%, the SiC codeposition value increased followed by a rapid decrease at higher D.C.s. There is an expected competition between SiC particles and
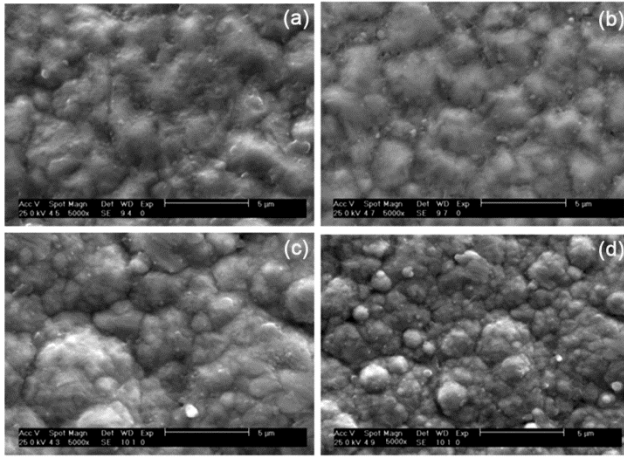
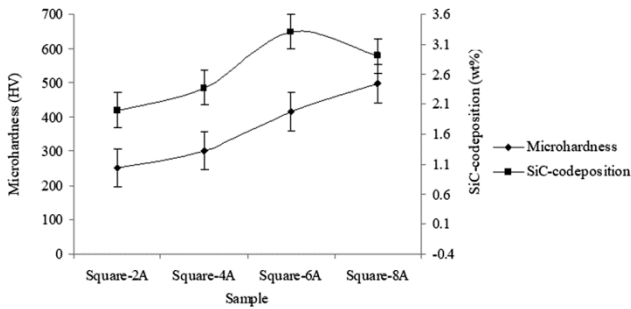Fig. 3 — The SEM micrographs of the coatings under different current densities (a) 2 A.dm^{-2}, (b) 4 A.dm^{-2}, (c) 6 A.dm^{-2} and (d) 8 A.dm^{-2}.

Fig. 4 — The microhardness and SiC-code position of the coatings under different current densities.
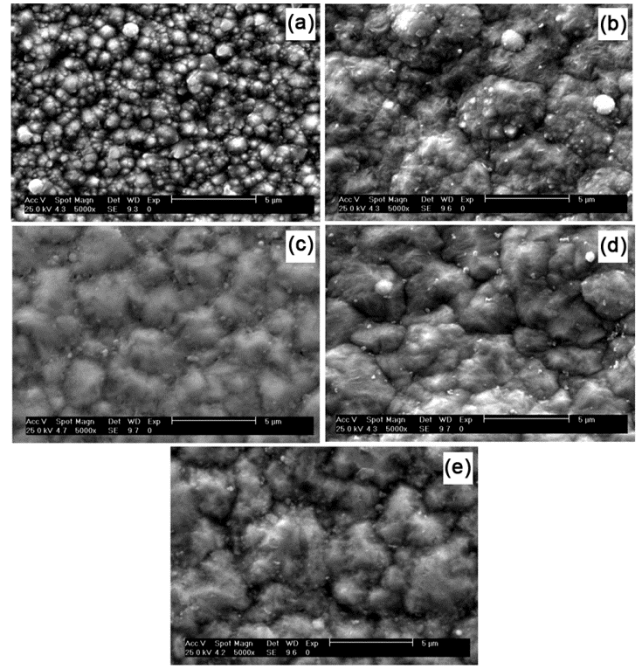

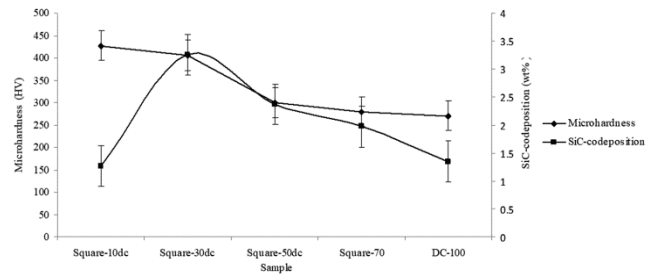Fig. 5 — The SEM micrographs of the coatings under different D.C.s (a) 10%, (b) 30%, (c) 50%, (d) 70% and (e) 100%.

Fig. 6 — The microhardness and SiC-code position of the coatings under different D.C.s.

nickel ions to deposit on the cathode surface. Inasmuch as electrophoresis forces are prominent during the on-time period, nickel ions have the higher chance to deposit on the cathode surface. Otherwise, at the off-time period, the electrophoresis forces do not work; therefore, nickel ions and SiC particles have the same chance to deposit on the cathode surface. According to Eq. (3) derived from Eq. (2), t_{off} and thereby the SiC code position decreased with the D.C.

$$t_{off} = (\frac{100\text{-}D.C.}{D.C.}) \cdot t_{on} \qquad \dots (3)$$

With regard to the above discussion, the result obtained at 10% D.C. is somewhat controversial and should be addressed. According to Guglielmi's adsorption mechanism, two steps contribute in deposition of a substance on the cathode surface. The first step is driven by loose physical adsorption of particles, which occurs during both off-time and on-time periods. The second step involves strong adsorption of particles due to electrochemical reaction during the on-time period[25]. Therefore, when the D.C. decreases to very low values, such as 10% in Fig. 6, there would not be sufficient on-time period for strong adsorption of particles on the cathode surface. For this reason, weak adsorbed particles on the cathode surface are removed during the next off-time period because of agitation and therefore, the code position of SiC particles decreases.

Figure 6 shows the microhardness results of the coatings obtained at different D.C.s. As clearly shown, the microhardness decreased with increase in the D.C. Increase in the microhardness at lower D.C. values can be attributed to finer grain microstructure and higher SiC code position. Also coarse grain

microstructure and lower SiC code position at higher D.C. values are responsible for the lower microhardness of the coatings. It is also important to note that although the value of the SiC code position at 10 % D.C. is very low, the effect of very fine grain microstructure is prominent and considerable microhardness can be justified accordingly.

3.3 Effect of Waveform on Microstructure, SiC-code position and Hardness

The charge value passing through the circuit during one cycle (also charge on the cathode surface) can be obtained according to Eq. (4), as follows:

$$q = \int_0^{\frac{T}{2}} i\,dt \qquad \qquad \ldots (4)$$

where, i, t and T are current, time and duration time of a cycle, respectively. SEM micrographs of the coatings performed by different waveforms are shown in Fig. 7. Considering the SEM micrographs, it can be easily concluded that the grain microstructure continues to become finer from the square waveform to sine and ramp waveforms. The reason for this is the higher charge value in order of square, sine and ramp, which is demonstrated parametrically in Table 5. The higher charge value leads to the reduction of the high amount of the nickel ions, which results in the grain growth of the nickel.

Figure 8 shows variations in the amount of the SiC code posited particles in the coatings at different waveforms. It is observed that the SiC code position decreased with changing the waveform from square to sine and ramp. As it is noted before, the code position process is under charge transfer control up to current
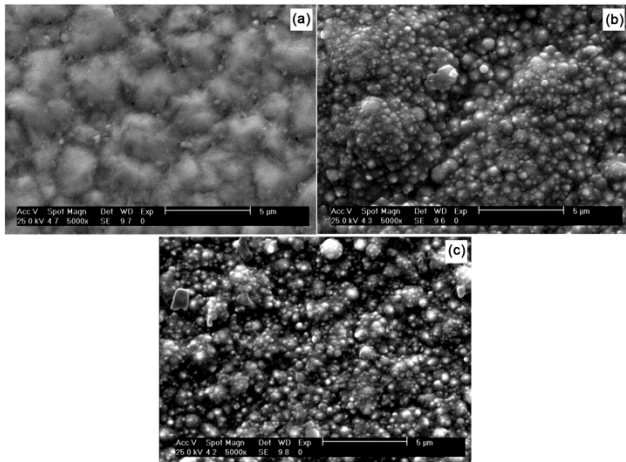
density of 6 A.dm^{-2} and above the current density of 6 A.dm^{-2}, the code position process is under mass transfer control. Thus, The SiC code position process is under charge transfer control at current density of 4 A.dm^{-2}. Considering Fig. 8, it is obvious that the waveform with higher charge value results in higher SiC code position. This is because higher charge value on the cathode surface leads to the reduction of the high amount of encircled ions of the SiC particles, and thereby to strong adsorption of higher amount of the SiC particles. Therefore, square waveform brings about higher SiC codeposition while ramp waveform causes lower SiC code position.

The results of the microhardness measurements in Fig. 8 illustrate that the coating hardness increases with changing the waveform in the order of square, sine and ramp. The reason for this is simply implied from difference in the grain microstructure of the coating obtained at each condition. According to the well-known Hall-Petch relation, finer grain structure leads to higher hardness. Although dispersion hardening is a strengthening mechanism, the reverse relation between the microhardness results and SiC codeposition values signifies that the Hall-Petch effect of the grain microstructure is the dominant strengthening mechanism in the microhardness changes.

Table 5 — The charge value at one cycle of different waveforms.

Waveform	Charge value (parametric)
Square	$\dfrac{i_p T}{2}$
Sine	$\dfrac{i_p T}{\pi}$
Ramp	$\dfrac{i_p T}{4}$

Fig. 7 — The SEM micrographs of the coatings under different waveforms (a) square, (b) sine and (c) ramp.
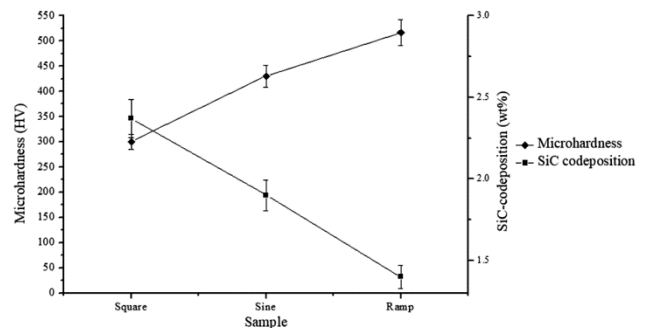

Fig. 8 — The microhardness and SiC-code position of the coatings under different waveforms.

4 Conclusions

Nickle/nano-SiC composite coatings were electrodeposited by the PDC. The effect of the current density, D.C. and waveform on the microstructure, microhardness and SiC code position was investigated. In summary, the following results could be mentioned.

(i) Higher current density resulted in finer grain microstructure, and subsequently in higher microhardness of the coatings. There were two controller processes: (a) charge transfer control up to 6 A.dm^{-2}, the increase of which in the current density led to higher SiC code position and (b) mass transfer control above 6 A.dm^{-2}, the increase of which in the current density caused lower SiC code position.

(ii) Lower D.C. led to finer grain microstructure and resulted in higher microhardness of the coatings. Moreover, lower D.C. brought about higher SiC code position. This is because lower D.C., i.e. higher t_{off} increased the chance of the SiC code position. However, this rule is not true at 10% D.C., which can be attributed to the insufficient on-time periods for strong adsorption of the SiC particles.

(iii) Changing the waveform from square to sine and ramp made the grain microstructure finer and resulted in higher microhardness. The lowest SiC code position of the ramp waveform can be ascribed to the lower charge value.

Acknowledgement

References

1 Heidari G, Tavakoli H & Khoie S M, *J Mater Eng Perform*, 19 (2010) 1183.
2 Singh K & Dwivedi C S, *Indian J Eng Mater Sci*, 8 (2001) 22.
3 Bikash P & Prasanta S, *Indian J Eng Mater Sci,* 22 (2015) 503.
4 Zheng X M, Zhang P Y, Wang L K, Tao S, Wang Y X, Huang L, Li J T & Sun S G, *Electrochimica Acta*, 247 (2017) 314.
5 Zheng X M, Xiao Y, Huang L, Ke F S, He Y, Li J T, Wei G Z & Sun S G, *Electrochem Commun*, 11 (2009) 1803.
6 Lajevardi S & Shahrabi T, *Appl Surf Sci*, 256 (2010) 6775.
7 Sen R, Das S & Das K, *Mater Character,* 62 (2011) 257.
8 Huang J M, Li Y, Zhang G F, Hou X D & Deng D W, *Surf Eng*, 29 (2013) 194.
9 Wang W, Hou F Y, Wang H & Guo H T, *Scripta Materialia*, 53 (2005) 613.
10 Sun W C, Zhang P, Zhao K, Tian M M & Wang Y, *Wear*, 342–343 (2015) 172.
11 Prasad P B S N V, Vasudevan R & Seshadri S K, *Indian J Eng Mater Sci*, 1 (1994) 158.
12 Gupta R N, Das A K, Nagahanumaiah & Henal S, *Mater Manuf Process*, 31 (2016) 42.
13 Boonyongmaneerat Y, Saengkiettiyut K, Saenapitak S & Sangsuk S, *J Alloys Comp,* 506 (2010) 151.
14 Jeon Y S, Byun J Y & Oh T S, *J Phy Chem Solids*, 69 (2008) 1391.
15 Khazrayie M & Aghdam A, *Transac Nonferrous Met Soc China*, 20 (2010) 1017.
16 Nickchi T, Ghorbani M, Alfantazi A & Farhat Z, *Mater Des*, 32 (2011) 3548.
17 Szeptycka B, Gajewska-Midzialek A & Babul T, *J Mater Eng Perform*, 25 (2016) 3134.
18 Zhang X, Qin J, Das M K, Hao R, Zhong H, Thueploy A, Limpanart S, Boonyongmaneerat Y, Ma M & Liu R, *Scientific Reports*, 6 (2016) 22285.
19 Zhou Y R, Zhang S, Nie L L, Zhu Z J, Zhang J Q, Cao F H & Zhang J X, *Transac Nonferrous Met Soc China*, 26 (2016) 2976.
20 Iacovetta D, Tam J & Erb U, *Surf Coat Technol*, 279 (2015) 134.
21 Aruna S, Bindu C, Selvi V E, Grips V W & Rajam K, *Surf Coat Technol*, 200 (2006) 6871.
22 Elkhoshkhany N, Hafnway A & Khaled A, *J Alloys Comp,* 695 (2017) 1505.
23 Gyftou P, Pavlatou E & Spyrellis N, *Appl Surf Sci*, 254 (2008) 5910.
24 Hu F & Chan K, *Appl Surf Sci*, 243 (2005) 251.
25 Wang S C & Wei W C J, *Mater Chem Phy*, 78 (2003) 574.